IEEE Access
Multidisciplinary | Rapid Review | Open Access Journal

Received March 27, 2020, accepted April 6, 2020, date of publication April 10, 2020, date of current version April 27, 2020.

*Digital Object Identifier 10.1109/ACCESS.2020.2987069*

# Analysis of a Fault-Tolerant Module-Combined Stator Permanent Magnet Synchronous Machine

**BINGYI ZHANG, BAOPING GAN, AND QIAOSHAN LI**
School of Electrical Engineering, Shenyang University of Technology, Shenyang 110870, China
Corresponding author: Baoping Gan (ganbaopingsteven@163.com)

**ABSTRACT** To solve the problems of large-size machining and complex control of fault-tolerant permanent magnet machines, a module-combined stator permanent magnet synchronous machine is proposed in this paper. The winding of the module-combined stator has two forms: large and small spans. The independent power supply of each module is adopted to decouple the electricity between each module, which enhances the manufacturing flexibility and the fault-tolerant ability of the motor. A mathematical model of the module-combined stator permanent magnet synchronous machine is established, and the design method of the machine is summarized. Then the analytical formula of the radial force acting on the stator under asymmetric operation is deduced. In addition, the torque-angle characteristics of the machine and the factors affecting the radial force are studied. Finally, the machine is prototyped, and both simulation and experiment are used verify the rationality of the proposed design.

**INDEX TERMS** Module-combined stator, asymmetric operation, torque-angle characteristic, fault-tolerant.

## I. INTRODUCTION

Low-speed and high-torque direct drive permanent magnet synchronous machines (PMSMs) can realize direct contact between power and load and offer the maximum energy transfer efficiency and are widely used in industrial production, wind power generation, ship propulsion and other fields [1]–[3]. The large volume of low-speed and high-torque PMSMs brings great difficulties in installation, manufacturing, transportation and maintenance. In special fields, higher requirements have been proposed for the fault tolerance of low-speed motors [4]–[6].

For traditional low-speed and high-torque motors, the stator is made by split lamination, and the stator core is processed as a whole, which is challenging because of its large volume. The winding of this kind of machine is usually slot concentrated winding [7], so the rotor and some adjacent windings must be removed during the maintenance of some windings of the machine, which is complicated and costly. At present, fault-tolerant motors mostly adopt multiphase vector decoupling control strategy and asymmetric decoupling fault-tolerant control technology for phase absence faults [8]–[10].

In Ref. [11], two fault-tolerant current control strategies are proposed for a nine-phase flux switching permanent magnet (FSPM) machine. The motor can still operate normally when one or two phase windings are open. In Ref. [12], a current vector fault-tolerant control strategy for a dual winding PMSM is proposed, which makes the output torque of the motor the same when the winding is open or short circuited and reduces the torque ripple of the motor. A fault-tolerant control strategy of a five-phase permanent magnet synchronous motor is studied in [13]. Based on the principle that the flux linkage of the permanent magnet remains unchanged, a nonlinear current control strategy of sliding mode control is proposed, which has good dynamic performance and tracking accuracy. In Ref. [14], a dual fault-tolerant control strategy is proposed to maximize the output torque and minimize the copper loss of the motor in the case of phase failure. The fixed frame fault-tolerant current control method is used to obtain the optimal current control for the multiphase PMSM, which enables the motor to smoothly transition its working state in normal and fault conditions [15]. In Ref. [16], a stator field oriented fault-tolerant control strategy is adopted for a permanent magnet switched reluctance motor; that is, the q-axis current component of the motor armature remains unchanged after a fault, so that the output torque does not change and there is good dynamic performance in the case of a fault. A five-phase double stator tubular flux modulation fault-tolerant permanent magnet motor is studied in Ref. [17], and the fault tolerance capacity of the motor is enhanced by using a single-layer fractional slot concentrated winding

The associate editor coordinating the review of this manuscript and approving it for publication was Xiaodong Liang.


This work is licensed under a Creative Commons Attribution 4.0 License. For more information, see https://creativecommons.org/licenses/by/4.0/

and fault tolerance tooth. Reference [18] describes a permanent magnet auxiliary synchronous reluctance motor that adopts three independent three-phase windings and isolates the windings so as not to overlap; each three-phase winding is equipped with an independent inverter to enhance the fault tolerance of the motor; so that the motor has good operation performance under both open-circuit and short-circuit faults. A fault-tolerant control method of a hybrid excitation axial magnetic field switching permanent magnet motor is studied in Ref. [19], in which the number of rotor poles, the width of the permanent magnet and other variables are optimized to increase the self-induction of the motor. Combined with adjusting the excitation current, a fault-tolerant control method based on space vector PWM with minimum copper loss is proposed. Most of the fault-tolerant motors proposed in the above literature adopt multiphase complex control to improve the fault tolerance, which increases the difficulty of motor processing and control, and problems such as maintenance difficulties cannot be avoided when the multiphase fault-tolerant motor is shut down for maintenance.

Based on the context discussed above, this paper proposes a module-combined stator PMSM (MCS-PMSM), which realizes the modular production of the stator. The processing and transportation problems brought by the large volume of the stator of the low-speed and large-torque PMSM can be solved. The MCS provides mechanical decoupling between the modules. The electrical decoupling of each module is implemented by using a mixed winding with large and small spans. Each module is powered by an independent inverter. When one module fails, the rest of the modules can still supply power normally without being affected, and the whole machine can operate normally with strong fault-tolerant ability. In practical applications, we do not need to remove the rotor or fault-free modules of the MCS-PMSM during shutdown maintenance. It is necessary only to loosen the corresponding end fasteners of the failed module, dismantle it separately and replace it with an operational healthy module.

In this paper, the MCS structure is first introduced, and the MCS splitting rule and the design principle of an unequal span winding are studied. The mathematical equation of the MCS-PMSM is deduced in the d-q coordinate system. The design method of the MCS-PMSM is summarized. In the proposed machine, if one module fails to operate, other modules will operate in the overload condition, which will create unbalanced radial forces in the machine, increasing the torque ripple. To reduce the stator current when the motor is overloaded, the torque-angle characteristics of the machine are analyzed so that it can output the rated torque at the minimum current. Unbalanced radial force and torque ripple generated by open-circuit faults in some modules are investigated. Through the analysis, it is found that with additional fault modules, the motor torque ripple and unbalanced radial force increase, and the whole motor system can still operate.

Finally, a prototype is made, and FEM and experimental tests verify the effectiveness of the theoretical analysis.

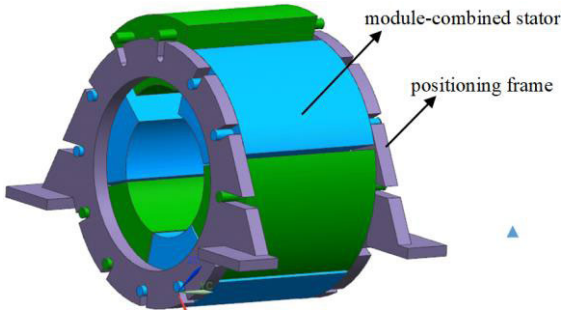


**FIGURE 1.** MCS-PMSM stator installation.

## II. MCS

### A. MCS CONFIGURATION

There is only one kind of span in the stator winding of the traditional motor; however, to modularize the stator, there are two kinds of span windings in each stator module of the MCS-PMSM: a large span and a small span. The large-span design ensures the independence of each module.

In the electrical field, the hybrid winding with large and small spans is exactly the same as the traditional winding, except that the end connection mode of the winding changes, as shown in Figs. 2 and 3.

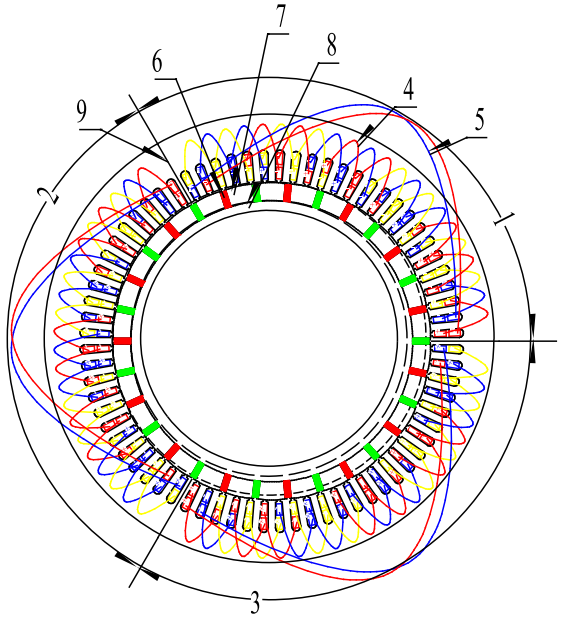


**FIGURE 2.** Windings of MCS-PMSM. (1-module 1 2-module 2 3-module 3 4-small span winding 5-large span winding 6-permanent magnet 7-magnetic pole 8-aluminum ring for magnetic isolation 9-position of module connection).

In this way, there is no winding across each module. Each module is powered independently to ensure electrical decoupling.

In the MCS, each module is equivalent to a stator running independently, which requires that each module meet the basic operation requirements of the stator of the rotating motor. For fractional slot winding motors, the greatest

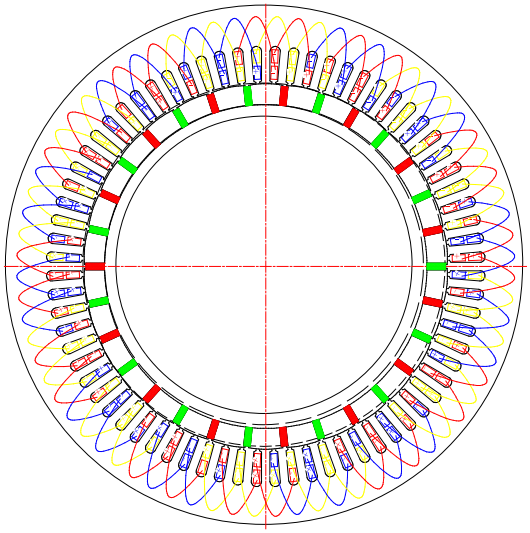

**FIGURE 3.** Windings of traditional PMSM.

common divisor $Z$ between the number of slots and the pole pairs is denoted as

$$Z = gcd(Q, P) \tag{1}$$

where gcd (**a**, **b**) represents the function for solving the greatest common divisor of **a** and **b**.

According to the theory of unit motors, it follows that

$$t = Z \tag{2}$$

$$Q_0 = \frac{Q}{t} \tag{3}$$

$$P_0 = \frac{P}{t} \tag{4}$$

where $t$ is the number of unit motors, $Q_0$ is the number of slots of the unit motor, and $P_0$ is the number of pole pairs of the unit motor. In the slot inductive EMF vector graph, there are $Q_0$ slots along the 360° circle, and the corresponding pole pairs is $P_0$. For a $Q$-slot, $P$-pole pair motor with unit motor number $t$, the slot inductive EMF vector graph is arranged repeatedly $t$ times.

Therefore, the split rule of the modular combined motor is as follows: the motor with $Q$ stator slots and $P$ polepairs can be split into $t$ modules at most, with $Q_0$ stator slots and $P_0$ pole pairs for each module, and the whole motor system can be powered by $t$ independent branches at most.

For motors with $Q$ slots, the slot pitch angle $\alpha$ is

$$\alpha = \frac{360^\circ}{Q} \tag{5}$$

The mechanical angle $\alpha_m$ occupied by the smallest modular motor in space is

$$\alpha_m = Q_0 \cdot \alpha = 360^\circ \frac{Q_0}{Q} \tag{6}$$

A motor with a stator slot number of $Q$ can be divided into $n$ modules. If the number of unit modules forming the $i$-th module is $k_i$, then the space angle $\alpha_i$ occupied by the $i$-th module can be given by

$$\alpha_i = k_i \cdot \alpha_m \tag{7}$$

The stator slots must be evenly distributed in the circumferential direction. Therefore, when splitting, the following conditions must be met:

$$\sum_{n}^{n} \alpha_i = 360^\circ \tag{8}$$

When $k_i = 1$, the unit module is a unit motor. In this case, the split is maximized.

According to winding theory, the span $y_1$ of the small-span winding of an independent motor module is

$$y_1 = \frac{5}{6}\tau = \frac{5}{6}\frac{Q}{2P} \tag{9}$$

According to the arrangement rules of MCS winding, the span $y_{2i}$ of the large-span winding in the $i$-th module is:

$$y_{2i} = k_i \cdot Q_0 - y_1 \tag{10}$$

When the number of unit modules that constitute the operation module is different, the span of the large-span winding of each operation module is also different, as is the space occupation angle of each module. Therefore, the inductance, resistance, magnetomotive force, output power and torque of each module are different.

The number of slots $q$ per pole per phase can be obtained by

$$q = \frac{Q}{2mp} \tag{11}$$

According to the above analysis, the above formula can be written as

$$q = \frac{Q_0}{2mP_0} \tag{12}$$

In the slot inductive EMF vector graph, the electrical phase shift $\alpha_p$ between two adjacent slots is calculated by

$$\alpha_p = P\frac{360^\circ}{Q} = 360^\circ \times \frac{P_0}{Q_0} = \frac{360^\circ}{2mq} \tag{13}$$

There is no common divisor between $Q_0$ and $P_0$ except 1. Eq. (12) shows that $q$ determines the ratio of $Q_0$ to $P_0$ under the condition of a certain number of motor phases.

In the process of motor design, $q$ influences the pole-slot matching directly. According to Eq. (13), when $q$ is fixed, the electric angle between adjacent EMF vectors in the slot inductive EMF vector graph is fixed, and different pole-slot matching means that the slot inductive EMF vector graph with the same phase is repeatedly arranged on the 360° circle.

Therefore, the number of slots per pole and phase determines the minimum number of slots and pole pairs required for the unit modular motor, while the pole-slot matching determines the maximum number of independent operation modules and the maximum number of power supply branches

**TABLE 1. Unit modular motor parameters with different $q$.**

| $q$ | 0.4 | 0.8 | 1.2 | 2 | 4 |
|---|---|---|---|---|---|
| $Q_0$ | 12 | 24 | 36 | 12 | 24 |
| $P_0$ | 5 | 5 | 5 | 1 | 1 |
| $y_1$ | 1 | 2 | 3 | 5 | 10 |
| $y_2$ | 11 | 22 | 33 | 7 | 14 |

of the whole motor system. The unit modular motor parameters with different $q$ values are shown in Table 1.

Table 2 lists the maximum number of branches of the MCS-PMSM under different pole-slot matching:

**TABLE 2. The maximum number of branches of the MCS-PMSM with different pole-slot matchings ($q = 0.8$).**

| $S/2P$ | 24/10 | 48/20 | 72/30 |
|---|---|---|---|
| the maximum number of branches | 1 | 2 | 3 |

### B. MATHEMATICAL MODEL OF THE MCS-PMSM

In the $d$-$q$ coordinate system, the excitation and torque components of the stator current can be decoupled to reflect the internal operation mechanism of the PMSM [20]. Therefore, the mathematical model of the MCS-PMSM is established in the $d$-$q$ coordinate system.

When all $n$ modules are put into operation, the voltage equation is

$$\begin{bmatrix} U_{d1} \\ U_{q1} \\ U_{d2} \\ U_{q2} \\ \vdots \\ U_{dn} \\ U_{qn} \end{bmatrix} = \frac{d}{dt}\begin{bmatrix} \psi_{d1} \\ \psi_{q1} \\ \psi_{d2} \\ \psi_{q2} \\ \vdots \\ \psi_{dn} \\ \psi_{qn} \end{bmatrix} - \omega\begin{bmatrix} \psi_{d1} \\ -\psi_{q1} \\ \psi_{d2} \\ -\psi_{q2} \\ \vdots \\ \psi_{dn} \\ -\psi_{qn} \end{bmatrix} + \begin{bmatrix} R_1 & 0 & 0 & 0 & 0 & \cdots & 0 \\ 0 & R_1 & 0 & 0 & 0 & \cdots & 0 \\ 0 & 0 & R_2 & 0 & 0 & \cdots & 0 \\ 0 & 0 & 0 & R_2 & 0 & \cdots & 0 \\ \vdots & \vdots & \vdots & \vdots & \vdots & \vdots & \vdots \\ 0 & 0 & 0 & 0 & 0 & R_n & 0 \\ 0 & 0 & 0 & 0 & 0 & 0 & R_n \end{bmatrix}\begin{bmatrix} i_{a1} \\ i_{q1} \\ i_{d2} \\ i_{q2} \\ \vdots \\ i_{dn} \\ i_{qn} \end{bmatrix} \tag{14}$$

where $U_{di}$ and $U_{qi}$ are respectively the $d$-axis and $q$-axis components of the stator voltage of the $i$-th module, $\psi_{di}$ and $\psi_{qi}$ are respectively the d-axis and q-axis components of the stator flux linkage of the $i$-th module, $i_d$ and $i_q$ are respectively the d-axis and q-axis components of the stator current of the $i$-th module, and $R_i$ is the phase resistance of the stator winding of the $i$-th module.

In particular, when the number of minimum unit modules comprising each operating module is the same.

The following equations can be obtained:

$$\left.\begin{array}{l} U_{d1} = U_{d2} = U_{d3} = \cdots = U_{dn} \\ U_{q1} = U_{q2} = U_{q3} = \cdots = U_{qn} \\ \psi_{d1} = \psi_{d2} = \psi_{d3} = \cdots = \psi_{dn} \\ \psi_{q1} = \psi_{q2} = \psi_{q3} = \cdots = \psi_{qn} \\ R_1 = R_2 = R_3 = \cdots = R_n \\ i_{d1} = i_{d2} = i_{d3} = \cdots = i_{dn} \\ i_{q1} = i_{q2} = i_{q3} = \cdots = i_{qn} \end{array}\right\} \tag{15}$$

The flux linkage equation can be given as

$$\begin{cases} \psi_{di} = L_{di} i_{di} + \psi_{fj} \\ \psi_{qi} = L_{qi} i_{qi} \end{cases} \tag{16}$$

where $\psi_{fi}$ is the flux linkage produced by the fundamental magnetic field of the permanent magnet in the stator winding of the $i$-th module.

For each operation module, the space angle occupied by each module is different when $k_i$ is different, as is the flux linkage in the stator winding of the module.

Torque and power equations

It is assumed that each independent operation module is powered by a three-phase symmetrical current, and the harmonic in the output current of the converter is not considered. Then, the torque equation of the MCS-PMSM can be expressed as

$$\begin{bmatrix} T_{em1} \\ T_{em2} \\ \vdots \\ T_{emn} \end{bmatrix} = P\left\{\begin{bmatrix} \psi_{d1} & 0 & \cdots & 0 \\ 0 & \psi_{d2} & 0 & 0 \\ \vdots & \vdots & \vdots & \vdots \\ 0 & 0 & \cdots & \psi_{dn} \end{bmatrix}\begin{bmatrix} i_{q1} \\ i_{q2} \\ \vdots \\ i_{qn} \end{bmatrix} - \begin{bmatrix} \psi_{q1} & 0 & \cdots & 0 \\ 0 & \psi_{q2} & \cdots & 0 \\ \vdots & \vdots & \vdots & \vdots \\ 0 & 0 & \cdots & \psi_{qn} \end{bmatrix}\begin{bmatrix} i_{d1} \\ i_{d2} \\ \vdots \\ i_{dn} \end{bmatrix}\right\} \tag{17}$$

where $T_{emi}$ is the output torque of the $i$-th module.

The output torque $T_{em}$ of the whole machine is

$$T_{em} = \sum_{i=1}^{n} T_{emi} \tag{18}$$

When the $i$-th module runs, the electromagnetic power $P_{emi}$ is

$$P_{emi} = T_{emi} \cdot \Omega \tag{19}$$

The electromagnetic power $P_{em}$ of the whole machine can be expressed as

$$P_{em} = \sum_{i=1}^{n} P_{emi} \tag{20}$$

According to the mathematical model of the MCS-PMSM, when $k_i$ is different, the angle occupied by each module in space and the parameters such as the inductance, resistance and flux linkage of each module are also different, as are the output torque and electromagnetic power distribution of

each module. For the whole machine, the distribution of each operating module on the circumference is asymmetric, so the whole machine can produce undesirable vibration, noise and output torque ripple, which affects the steady-state operation performance of the machine.

Therefore, it is essential that the $k_i$ values should be equal during splitting, ensuring that each operation module is exactly the same and distributed symmetrically in space. In this way, the MCS has no impact on the operation of the whole machine.

## III. DESIGN AND ANALYSIS OF MCS-PMSMS

### A. ROTOR STRUCTURE OF THE MCS-PMSM

The mechanical motion equation of the PMSM is [21]

$$T_{em} = J\frac{d\Omega_r}{dt} + R_\Omega \Omega_r + t_L \tag{21}$$

where $T_{em}$ is the electromagnetic torque, $T_L$ is the load torque (including the no-load torque of the motor), $\Omega_r$ is the mechanical angular speed of the rotor, $J$ is the moment of inertia of the system, and $R_\Omega$ is the damping coefficient.

The output power of the motor system will be reduced if some modules fail. Under the condition that the load remains unchanged, the torque output by other modules is bound to increase. At this time, the machine is essentially working in the overload state. If the overload capacity of the machine is insufficient, the machine will be out of step and cannot operate normally. Therefore, the fault-tolerant capacity of an MCS-PMSM is directly related to its overload capacity.

The torque $T_{em}$ of a PMSM can be calculated by

$$T_{em} = p\left[i_s\psi_f \sin\beta + \frac{1}{2}\left(L_d - L_q\right) i_s^2 \sin 2\beta\right] \tag{22}$$

where $i_s$ is the stator current in the $d$-$q$ coordinate system; $p$ is the number of pole pairs; $\psi_f$ is the permanent magnet flux linkage; $\beta$ is the angle between the current vector and $q$-axis in the $d$-$q$ coordinate system; and $L_d$ and $L_q$ are respectively the $d$-axis and $q$-axis inductances of the stator winding.

The output torque of the PMSM is composed of the permanent magnet torque and reluctance torque. The permanent magnet torque is determined by the air-gap flux generated by the permanent magnet. The reluctance torque is related to the rotor structure of the machine.

The common rotor structures of low-speed and high-torque PMSMs are surface mounted and tangentially embedded. The $d$-axis reactance is equal to the $q$-axis reactance in a surface-mounted PMSM, and the machine has no reluctance torque and a small magnetic flux leakage [22].

However, it is necessary to drill holes in the permanent magnets or press the strips on the permanent magnets while assembling permanent magnets, which causes damage to the permanent magnets and complicates the assembly process.

For the tangential embedded rotor, the air-gap flux generated by each magnetic pole is twice as much as that of the surface mounted rotor, and the reluctance torque is produced due to the asymmetry of the magnetic circuit of the $d$-axis and the $q$-axis, which is conducive to the operation of the low-speed and high-torque PMSM.

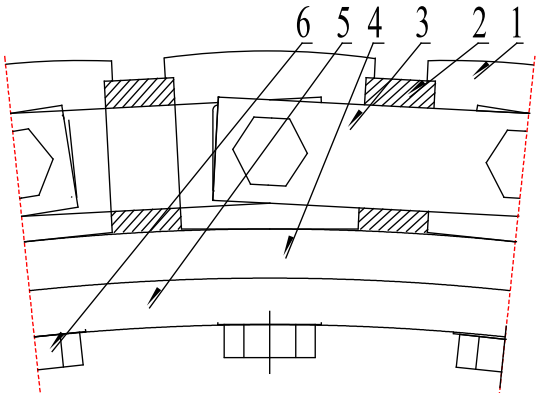


**FIGURE 4.** Tangentially Embedded Rotor Structure.(1-magnetic pole 2-permanent magnet 3-permanent magnet baffle 4- aluminum ring for magnetic isolation 5- supporting ring 6 -bolt).

A novel tangential rotor structure is proposed in this paper. The magnetic poles of the tangential rotor are superimposed by punches that can be made for uneven air gaps to improve the air-gap density waveform. During the process of rotor assembly, the rotor magnetic poles are fixed with the magnetic separator ring and the rotor support ring, and then the permanent magnets are inserted into the middle of the two adjacent magnetic poles. To prevent the permanent magnets from moving along the axial direction, the baffles are fixed on the two adjacent magnetic pole diagonal tension screws.

When the motor is running, the time harmonics caused by the change in the air-gap permeance, the nonsinusoidal power supply and the space harmonics caused by the distributed winding all lead to eddy current loss in permanent magnets [23]. Permanent magnets are irreversibly demagnetized if the temperature is too high [24].

When the machines with two kinds of rotor structures output the rated torque, the eddy current loss of the permanent magnets is as shown in Figs. 5 and 6.

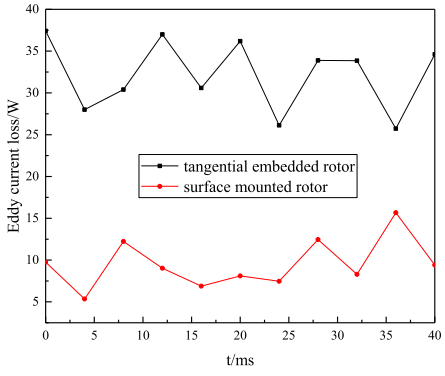


**FIGURE 5.** Eddy current loss of permanent magnet with different rotor structures.

As shown in Fig. 5, the eddy current loss of the surface mounted rotor is approximately 4 times that of the tangential

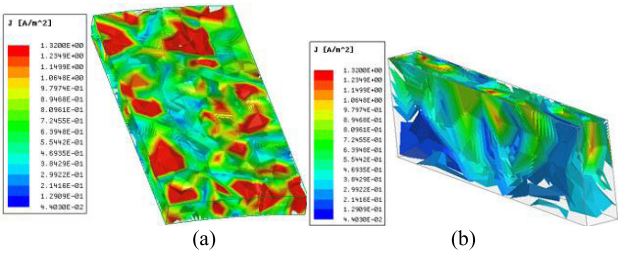


**FIGURE 6.** Eddy current density. a. Surface mounted rotor b. Tangentially.

embedded structure. As shown in Fig. 6, the eddy current density on the surface of the permanent magnets of the surface mounted rotor is larger than that on the tangential embedded rotor. Therefore, the tangential embedded rotor is selected in this paper.

### B. MCS-PMSM DESIGN

An MCS-PMSM is different from a traditional PMSM only in the connection mode of the stator winding end. Therefore, the basic magnetic circuit calculation method of the conventional motor is still applicable to the design of the MCS-PMSM. In this paper, first, the basic magnetic circuit calculation method is used to transform equivalent multiple modular motors into a whole motor, and the FEM is used to verify the solution. Then, the whole motor is divided into modular motors according to the modular stator separation rules and the MCS-PMSM mathematical model. Finally, the performance of the MCS-PMSM is analyzed by the FEM under both healthy conditions and fault conditions.

It is difficult for the rotor to dissipate heat, and the temperature of the rotor rises during long-term operation. The material of MCS-PMSM permanent magnets is NdFeB with a high temperature coefficient. With increasing temperature, the load operation point of the permanent magnet decreases, the rotor magnetomotive potential decreases, the stator current of the motor increases, and then the motor loss increases. The increase in motor loss further causes a rise in the rotor temperature. Once the load operation point of a permanent magnet is lower than the inflection point, the magnet is irreversibly demagnetized. Therefore, special attention should be paid to the motor operating temperature in the design of fault-tolerant motors. In the design of the traditional PMSM, the working temperature is first estimated. After the electromagnetic design, the motor loss is calculated according to the operating parameters of the motor at the estimated temperature. Finally, the actual motor temperature can be obtained in the temperature field on the basis of the calculated loss. However, this is a one-way coupling calculation method from the electromagnetic field to the temperature field. This method cannot take into account the influence of a large error between the estimated temperature and calculated temperature on the motor loss and temperature calculation. In addition, the MCS-PMSM may work in an overload state during fault operation, and the parameters of the motor

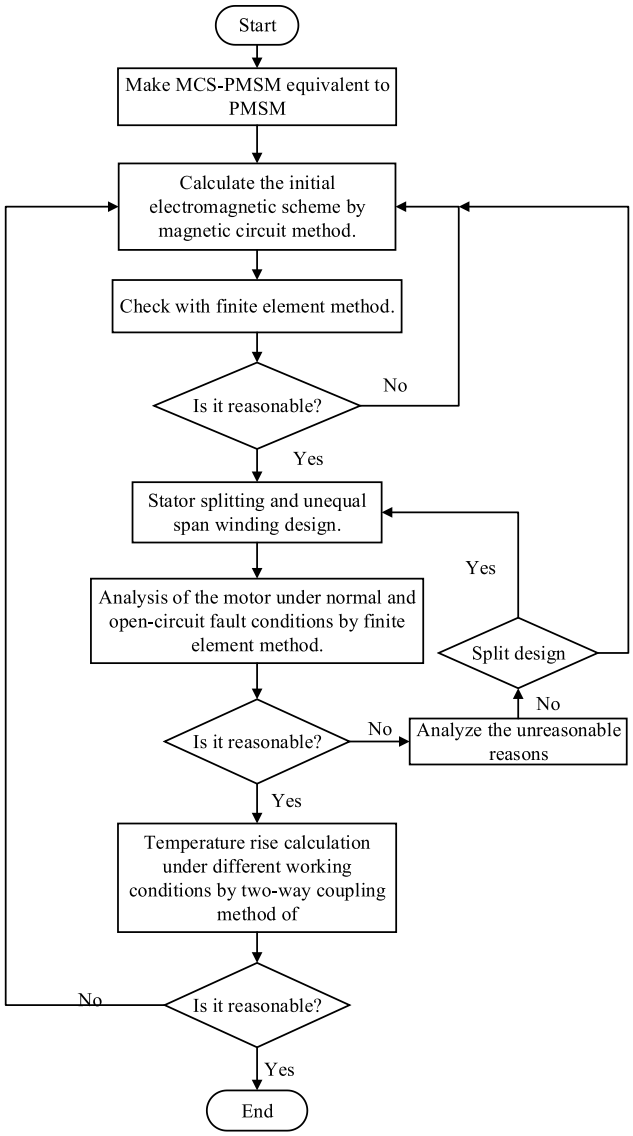


**FIGURE 7.** MCS-PMSM design process.

magnetic circuit and temperature will interact, so the traditional temperature calculation method is no longer applicable to the design of the MCS-PMSM.

Therefore, a calculation method of adding a temperature check cycle to the traditional magnetic circuit calculation method is proposed in this paper. Considering the mutual influence of the temperature field and electromagnetic field, the two-way coupling calculation method of the electromagnetic field and temperature field is used to calculate the performance of the motor under different working conditions. The MCS-PMSM design process is as follows:

According to the above design process, an MCS-PMSM is designed. The basic parameters of the prototype are shown in Table 3:

### C. HEALTHY CONDITION

The no-load back EMF of the PMSM plays a crucial role in the steady-state operation of the motor. The no-load back

**TABLE 3. Parmeters of MCS-PMSM.**

| Parmeter | Value |
|---|---|
| Rated power/kw | 12 |
| Rated speed/(r/min) | 100 |
| Rated frequency/Hz | 25 |
| Rated voltage(V) | 380 |
| Slot/pole | 72/30 |
| Air-gap flux density/T | 0.823 |
| Stator core length/mm | 220 |
| No-load back EMF/V | 208.5 |
| Number of modules | 3 |
| Small span | 2 |
| Large span | 22 |

EMF of the MCS-PMSM calculated by the FEM is shown in Fig. 8, and the effective value is 210.2 V. The error of the result calculated by the magnetic circuit method is only 1.7 V, which proves the accuracy of the magnetic circuit method. The no-load back EMF is decomposed by the FFT, and the THD is 5.56%.

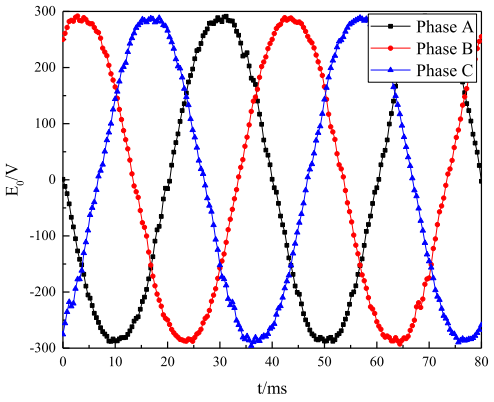


**FIGURE 8. No-load back EMF of the MCS-PMSM.**

Low-speed and high-torque motors are often operated with constant torque. The higher no-load back EMF and the lower THD can reduce the no-load loss and torque ripple of the machine, and the power factor can also be improved.

Three modules of the investigated machine arepowered with symmetrical three-phase current under healthy conditions, and the output torque of the motor is shown in Fig. 9. The output torque of the motor is stable when the parameters of each module are the same, and the torque ripple is only 0.94%.

Fig. 10 compares the armature flux line distribution of the ordinary PMSM and the MCS-PMSM under the same excitation. The results show that the MCS-PMSM generates a 30-pole magnetic field at a circumference of 360°, exactly the same as the ordinary PMSM. That is, the MCS and large- and small-span hybrid windings have no effect on the whole motor system.

The torque-angle characteristics play an important role in PMSMs [25]. The torque-angle characteristic can reflect the change in the output torque caused by a change in the current vector angle (the angle between the stator current vector and *d*-axis positive direction) when the stator current is fixed.

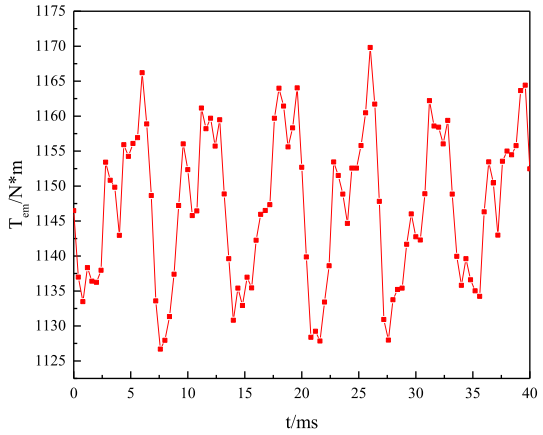


**FIGURE 9. Output torque of the MCS-PMSM.**

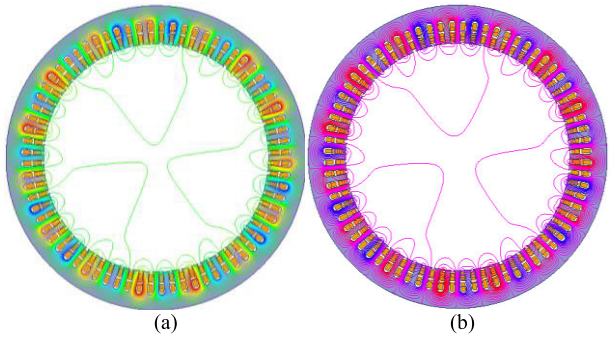


**FIGURE 10. Flux line distribution. a. Common PMSM. b. MCS-PMSM.**

By taking into account the maximum output current of the controller, the maximum output torque of the motor can be calculated by using the torque-angle characteristic to better evaluate the operation performance of the motor.

The torque-angle characteristic plays an important role in PMSMs [25]. The torque-angle characteristic can reflect the change of output torque caused by the change of current vector angle (the angle between stator current vector and *d*-axis positive direction) when the stator current is fixed. Taking into account the maximum output current of the controller, the maximum output torque of the motor can be calculated by using the torque-angle characteristic, so as to evaluate the operation performance of the motor better.

To illustrate the torque-angle characteristics of the embedded tangential PMSM, the maximum operating current of the motor is determined to be 2 times the rated current. With the frozen permeability method in Ref. [26], the torque-angle characteristics of the motor are obtained by separating the permanent magnet torque and the reluctance torque. The torque-angle characteristics of the motor at the rated current and 2 times the rated current are calculated by the FEM, as shown in Fig. 11 and Table 4.

From the above analysis, it can be concluded that the phase current angle is relatively small when the motor outputs the maximum torque at the rated current, and the ratio of the reluctance torque to the maximum torque is also very small.

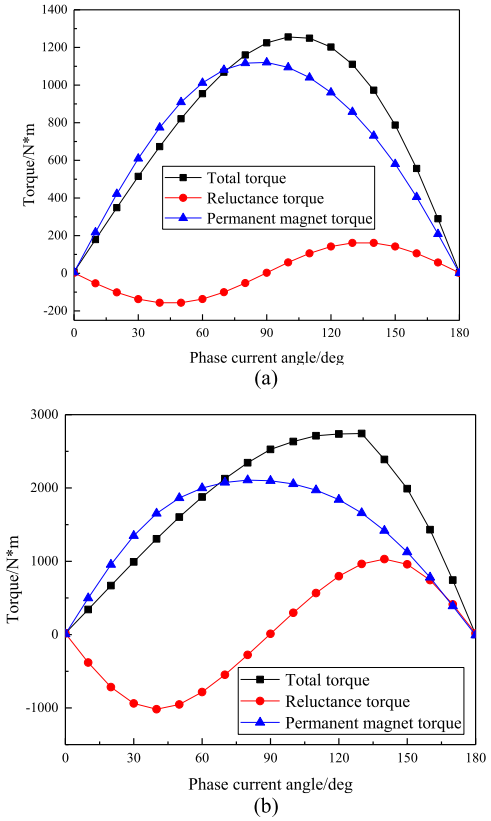


**FIGURE 11.** Torque-angle characteristics. a. Rated current. b. 2 times of the rated current.

**TABLE 4.** Torque-angle characteristics.

A. RATED CURRENT

| Parameter | Value |
|---|---|
| Rated torque(N*m) | 1145.7 |
| Rated torque-phase current angle(deg) | 97.85 |
| Maximum torque(N*m) | 1251.7 |
| Maximum torque-phase current angle(deg) | 108 |
| Reluctance torque at rated torque(N*m) | 10.78 |
| Maximum reluctance torque(N*m) | 161.32 |
| Reluctance torque at rated torque/rated torque | 5% |

B. 2 TIMES OF THE RATED CURRENT

| Parameter | Value |
|---|---|
| Maximum torque(N*m) | 2749.68 |
| Maximum torque-phase current angle(deg) | 130.1 |
| Maximum reluctance torque(N*m) | 1030.5 |
| Maximum torque multiple | 2.4 |
| Reluctance torque at Maximum torque / Maximum torque | 30% |

When the current increases, the angle of the phase current increases, as does the ratio of the reluctance torque to the maximum torque.

The reason is that the permanent magnet torque is related to the product of the phase current, and the reluctance torque is related to the square product of the phase current. At the rated current, the output reluctance torque of the motor is small, and the maximum torque of the motor depends on the maximum permanent magnet torque. When the current increases, the output reluctance torque increases, and the maximum torque of the motor depends on the maximum value of the sum of the reluctance torque and the permanent magnet torque. Therefore, the stator phase current angle and the proportion of the reluctance torque both increase when the maximum torque of the motor is output.

According to the above analysis, when an open-circuit fault occurs in some module windings, the MCS-PMSM can make full use of the reluctance torque of the tangential embedded rotor to ensure the normal operation of the system.

## IV. FAULT TOLERANCE ANALYSIS

### A. FAULT TOLERANCE PRINCIPLE OF MCS

In the MCS-PMSM, the mechanical decoupling of the stator is realized via the stator modular, and the electrical decoupling among the modules is realized by the large- and small-span hybrid windings and independent power supply. When a module fails, the fault unit and its controller can directly be cut off as a whole, and the other modules can still operate normally without being affected. Since each running module is composed of a unit motor, which is equivalent to an independent running motor, the current phase in the remaining windings can still operate normally without readjustment.

### B. RADIAL FORCE OF MCS-PMSM UNDER FAULT CONDITION

To ensure the stability of motor operation, each operation module $k_i$ is taken as equal. According to Eq. (17),

$$T_{em} = np\left(\psi_d i_q - \psi_q i_d\right) \tag{23}$$

If the $d$-axis and $q$-axis current of the fault module in the current matrix is set to 0, Eq. (17) is still applicable when some modules fail. It can be deduced that when there are $k$ modules working, the output torque of the motor can be obtained by

$$T_{em} = kp\left(\psi_d i_q - \psi_q i_d\right) \tag{24}$$

The above expression shows that when each module is identical, the output torque of the motor is related only to the number of modules put into operation, regardless of the location of the module.

When some modules of the MCS-PMSM fail, an asymmetric magnetic field results in a radial force. In this section, the unbalanced radial force is calculated by the Maxwell tensor method with an ideal simplified model. Some assumptions are made as follows:

1. The saturation of the air-gap magnetic field is ignored;
2. Regardless of rotor eccentricity, the surface of the stator and rotor is smooth.

For module $i$, the three-phase symmetrical winding is powered by a symmetrical three-phase current to generate a

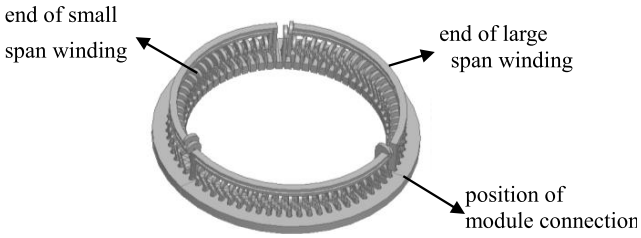


**FIGURE 12.** MCS winding end connection diagram.

magnetic EMF $f_{si}$, and the $f_{si}$ can be expressed as [27]

$$f_{si}(\theta,t)=\begin{cases}\sum \dfrac{3\sqrt{2}Nk_{iw}}{\pi p}I_i\cos(\omega t-vp\theta) & v=6k-5\\ \sum \dfrac{3\sqrt{2}Nk_{ix}}{\pi p}I_i\cos(\omega t+vp\theta) & v=6k-1\\ k=1,2,3\cdots\end{cases} \tag{25}$$

where $N$ is the number of turns-in-series per phase of the stator, $K_{wv}$ is the winding coefficient of the $v$-harmonic magnetomotive force, $\omega$ is the angular frequency, $p$ is the number of pole pairs, and $I_i$ is the phase current effective value of the $i$-th module.

The magnetic field produced by permanent magnets of the MCS-PMSM is not sinusoidal. According to the magnetic circuit analysis principle of the PMSM, the rotor permanent magnet magnetomotive force is composed of a series of $\mu$-th harmonic magnetomotive forces, which is expressed as

$$f_r(\theta,t)=\sum F_\mu\cos(\mu\omega t-\mu p\theta)\quad \mu=2k+1\ k=0,1,2\cdots \tag{26}$$

The air-gap permeance is

$$\Lambda(\theta,t)=\Lambda_0+\sum_{k=1}^{\infty}\Lambda_k\cos(kZ\theta) \tag{27}$$

According to the Maxwell tensor method, the radial electromagnetic force density acting on the inner surface of the stator core is [28]:

$$p_r=\frac{1}{2\mu_0}\left(B_r^2-B_t^2\right)\approx\frac{1}{2\mu_0}B_r^2 \tag{28}$$

On the basis of the superposition principle, the air-gap flux density of the $i$-th module can be calculated as

$$B_i(\theta,t)=(f_{si}(\theta,t)+f_r(\theta,t))\,\Lambda(\theta,t) \tag{29}$$

The air-gap flux density of each stator module is the same because each stator module is identical.

To simplify the analysis, it is assumed that the number of stator modules is even. The $i$-th module is faulty, and the $j$-module is opposite to it. Fig. 13 shows the radial force acting on the two modules.

Since the number of stator modules is assumed to be even, the remaining modules are symmetrically distributed in space, and the radial resultant force is 0.

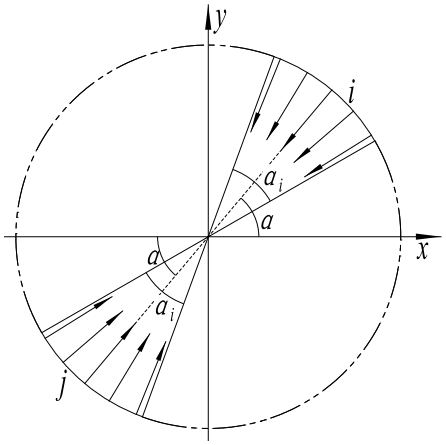


**FIGURE 13.** The radial force distribution when a module fails.

According to the symmetry, the values of the radial force density of the $i$-th module and the $j$-th module are exactly the same, and only the direction of the force is different.

The radial force density in the $x$ and $y$ directions are

$$\begin{cases}p_{rxi(j)}=p_{ri(j)}\cos\alpha\\ p_{ryi(j)}=p_{ri(j)}\sin\alpha\end{cases} \tag{30}$$

The radial forces in the $x$ and $y$ directions are:

$$\begin{cases}F_{xi(j)}=\int_S p_{rxi(j)}dS=C\int_0^{\alpha_i}p_{ri(j)}\cos\alpha d\alpha\\ F_{yx(j)}=\int_S p_{ryi(j)}dS=C\int_0^{\alpha_i}p_{ri(j)}\sin\alpha d\alpha\end{cases} \tag{31}$$

where $C$ is related to the size of the motor, which is, $D_i$ is the inner diameter of the stator; and $l_{ef}$ is the length of the stator core.

The unbalanced radial force in the $x$ and $y$ directions is

$$\begin{cases}\Delta F_x=F_{xj}-F_{xi}=C\int_0^{\alpha_i}\left(p_{rj}-p_{ri}\right)\cos\alpha d\alpha\\ \Delta F_y=F_{xj}-F_{yi}=C\int_0^{\alpha_i}\left(p_{ij}-p_{ri}\right)\sin\alpha d\alpha\end{cases} \tag{32}$$

When the i-th module fails, its stator current $I_i = 0$. In the fault area, the air-gap magnetic field is generated by permanent magnets only. The radial force density in the x and y directions is obtained as follows:

$$\begin{aligned}\Delta p_{rx}&=\frac{1}{2\mu_0}\Lambda^2(\theta,t)\left[f_{sj}^2(\theta,t)+2f_r(\theta,t)f_{sj}(\theta,t)\right]\cos\alpha\\ \Delta p_{ry}&=\frac{1}{2\mu_0}\Lambda^2(\theta,t)\left[f_{sj}^2(\theta,t)+2f_r(\theta,t)f_{sj}(\theta,t)\right]\sin\alpha\end{aligned} \tag{33}$$

Eq. (33) shows that the unbalanced magnetic force is caused by the stator magnetic field interaction with the fault module and the stator and rotor magnetic field interaction. Because the two modules are opposite and identical, the rotor magnetic field interaction cancels out.

The expressions of the magnetomotive force and air-gap permeability of the stator and rotor are introduced into

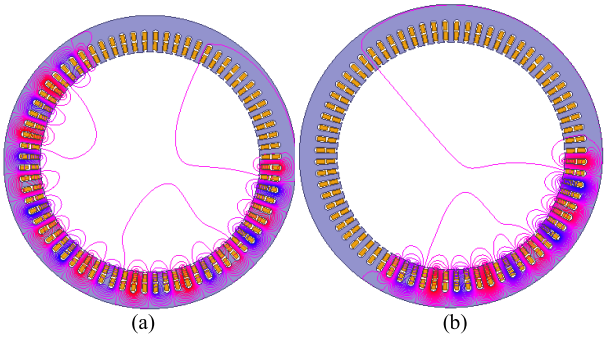


**FIGURE 14.** Distribution of the armature flux line.(a) Open-circuit fault in one module. (b) Open-circuit fault in two modules.

Eqs. (32) and (33) to obtain the unbalanced radial force as given by Eq. (34), as shown at the bottom of this page.

In general, the radial force analysis method is the same as the above method under asymmetric operation conditions. First, the radial force density is decomposed into the $x$ and $y$ directions, and the radial force in the $x$ and $y$ directions is calculated along the circumference integral. Then, the radial resultant force is obtained according to the spatial distribution of the fault module.

The above analysis shows that when the motor parameters are fixed, the radial force generated by the asymmetric operation is related to the current during the normal operation of the motor, the angle occupied by the module in space, and the relative position of the fault module and the nonfault module.

The power of the whole motor system is $P_{em}$, the current is $I$, the area inside the stator is $S$, and the motor is divided into n identical modules. According to the mathematical equation of the modular motor, the rated current of each module is $I\ /\ n$, the space occupied angle of each module is $360°/n$, and the power of each module is $P_{em}/\ n$. When $n$ is larger, the power, current and space occupied angle of each module are smaller. According to Eq. (34), the radial force acting on the stator decreases when a module fails. According to the previous analysis, when the motor operates asymmetrically, the radial force of the stator and the electromagnetic power loss of the motor are the smallest in the case of $n = t$.

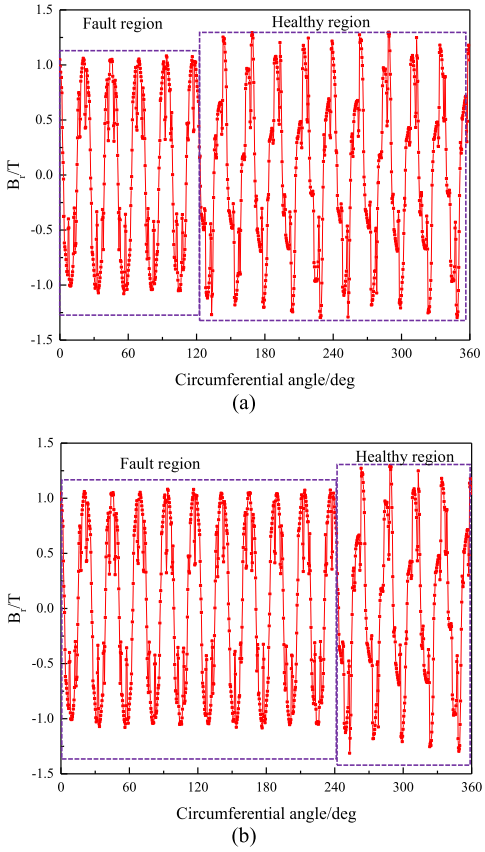


**FIGURE 15.** Air gap flux density under load condition. (a) Open-circuit fault in one module. (b) Open-circuit fault in two modules.

*Open-Circuit Fault:* The distribution of the armature flux line, the radial air-gap flux density and the output torque of the motor under the fault condition are obtained by FEM, as shown in Figs. 14-16.

$$
\begin{aligned}
F_x = \frac{C}{2\mu_0}\int_0^a \left[\Lambda_0 + \sum_{k=1}^{\infty}\Lambda_k \cos(kZ\theta)\right] \\
\times \left\{\begin{array}{l}\left[\sum \frac{3\sqrt{2}Nk_{wv}}{\pi p} I_i \cos(\omega t - vp\theta) + \sum \frac{3\sqrt{2}Nk_{wv}}{\pi p} I_i \cos(\omega t + vp\theta)\right] \\ +\ 2\sum F_\mu \cos(\mu\omega t - \mu p\theta)\left[\sum \frac{3\sqrt{2}Nk_{wv}}{\pi p} I_i \cos(\omega t - vp\theta) + \sum \frac{3\sqrt{2}Nk_{wv}}{\pi p} I_i \cos(\omega t + vp\theta)\right]\end{array}\right\} \cos\alpha d\alpha \\
F_y = \frac{C}{2\mu_0}\int_0^a \left[\Lambda_0 + \sum_{k=1}^{\infty}\Lambda_k \cos(kZ\theta)\right] \\
\times \left\{\begin{array}{l}\left[\sum \frac{3\sqrt{2}Nk_{wv}}{\pi p} I_i \cos(\omega t - vp\theta) + \sum \frac{3\sqrt{2}Nk_{wv}}{\pi p} I_i \cos(\omega t + vp\theta)\right] \\ +\ 2\sum F_\mu \cos(\mu\omega t - \mu p\theta)\left[\sum \frac{3\sqrt{2}Nk_{wv}}{\pi p} I_i \cos(\omega t - vp\theta) + \sum \frac{3\sqrt{2}Nk_{wv}}{\pi p} I_i \cos(\omega t + vp\theta)\right]\end{array}\right\} \sin\alpha d\alpha
\end{aligned}
\tag{34}
$$

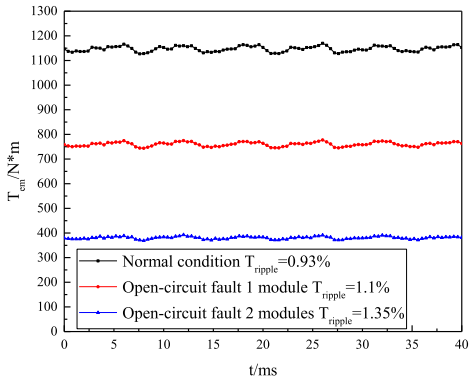


**FIGURE 16.** Output torque. 1- Healthy Operation. 2- Open-circuit fault in one module. 3- Open-circuit fault in two modules.

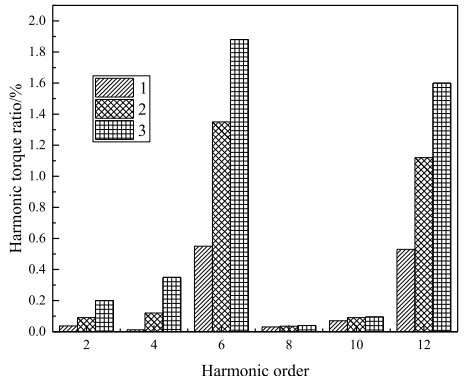


**FIGURE 17.** Torque harmonic. 1- Healthy Operation. 2- Open-circuit fault in one module. 3- Open-circuit fault in two modules.

According to the results in Figs.16, when one module fails, the average output torque of the motor is slightly lower than the rated torque by 2/3, and the output torque is slightly lower than the rated torque by 1/3 when two modules fail.

When some modules of the machine fail, the 2nd, 4th, 6th and 12th harmonic torques increase, as does the torque ripple.The torque ripple increases with the decrease in the number of modules put into operation, which is caused by the radial force generated by the unbalanced magnetic field due to the open-circuit fault of some modules.

The number of stator modules of the prototype is 3, and the radial force distribution is shown in Fig. 18.

The radial force of the MCS-PMSM with different numbers of fault modules is shown in Fig. 19. In the case of failure of one or two modules, the results of the radial force in the X direction calculated by the FEM are 0.74 N, and1.53 N the results calculated by the analytical method are 0.82 N and 1.62 N. For the radial force in the Y direction, the results calculated by the FEM are 1.39 N and 1.41 N, the results calculated by the analytical method are 1.44 N and 1.47 N. The numerical value calculated by the analytical method is slightly higher than that of the FEM. This is because the saturation effect is not taken into consideration in the analytical method.

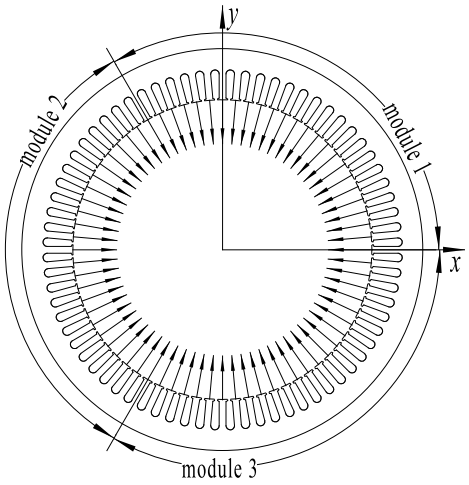


**FIGURE 18.** The radial force distribution of the prototype.

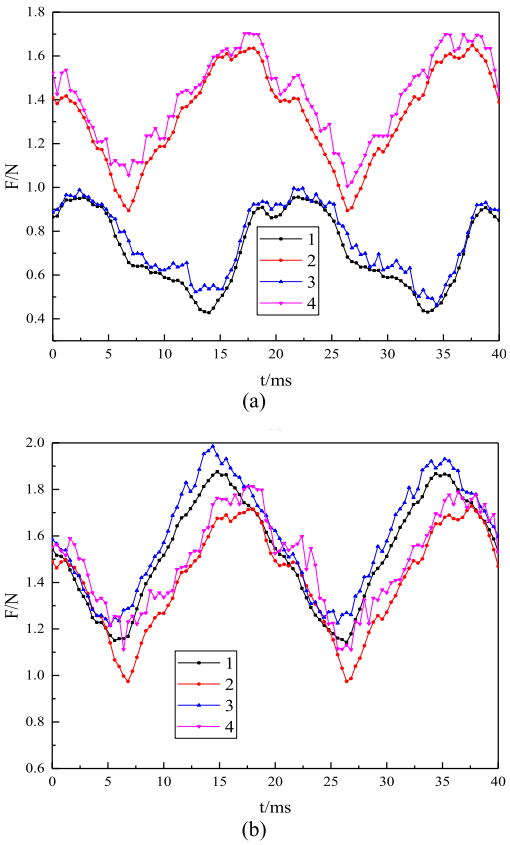


**FIGURE 19.** Radial force of the MCS-PMSM with different number of fault modules. (a) one fault module. (b) Two fault modules. 1- $F_x$FEM. 2-$F_y$FEM. 3-$F_x$ Analytical. 4- $F_y$ Analytical.

When some modules fail, the waveform and average value of the radial force in the Y direction are almost the same, and the radial force in the X direction becomes larger. According to Fig. 18, the reasons can be summarized as follows: the radial force of module 2 in the Y direction is 0, only the radial force in the X positive direction is generated, and

**TABLE 5. Torque characteristics with different numbers of modules at rated current.**

| | One fault module | Two fault modules |
|---|---|---|
| Input current | 1.42 times of rated current | 2.5 times of rated current |
| Generate rated torque current angle / deg | 110.5 | 136.6 |
| Reluctance torque (rated torque current angle) | 224.6 | 481.2 |
| Reluctance torque / rated torque (rated torque current angle) | 19.6% | 42% |

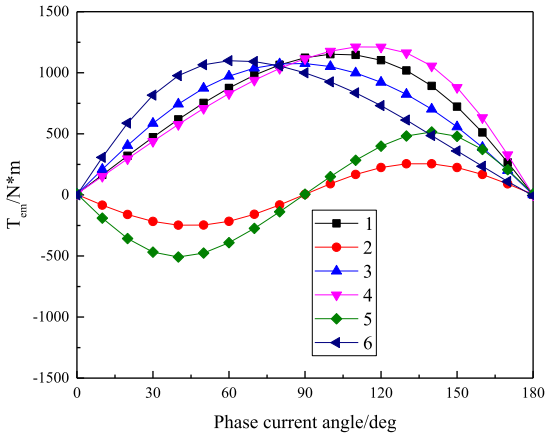


**FIGURE 20.** Torque-angle characteristic with different numbers of modules running. 1-Total torque when 2 modules work (1.42 times of rated current input). 2-Reluctance torque when 2 modules work (1.42 times of rated current input). 3-Permanent magnet torque when 2 modules work (1.42 times of rated current input). 4-Total torque when 1 module works (2.5 times of rated current input). 5-Reluctance torque when 1 module works (2.5 times of rated current input). 6-Permanent magnet torque when 1 module works (2.5 times of rated current input).

the radial force in the Y direction is determined by modules 1 and 3; therefore, the average value of the radial force in the Y direction is almost unchanged, and the radial force in the X direction increases when module 2 fails.

Fault-tolerant operation of MCS-PMSM means that other modules can still meet the normal operation of the load when some modules fail. Therefore, taking the rated output torque as the goal, the torque-angle characteristics of the motor are studied when one module and two modules fail, and the results are shown in Fig. 20.

According to the torque-angle characteristic curve obtained above, the output torque of the MCS-PMSM is calculated by the FEM when different number modules are put into operation. As shown in Fig. 21, the output torque and torque ripple of the motor increase with a decrease in the number of normal operation modules. In addition to the unbalanced radial force, the increase in the output reluctance torque also causes an increase in the torque ripple.

The torque characteristics with different numbers of fault modules are listed in Table 5.

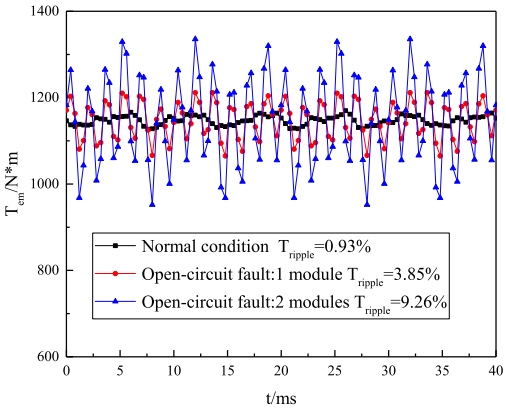


**FIGURE 21.** Output torque ripple of the MCS-PMSM.

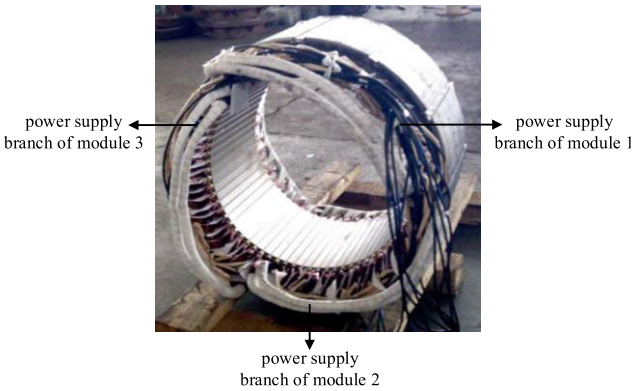


**FIGURE 22.** Stator of the prototype.

When one module and two modules fail, the stator current needs to be input to 1.42 times and 2.5 times the rated current, respectively, and then the motor can output the rated torque.

This is because the phase current amplitude and angle increase with the reduction in the number of modules put into operation when the rated torque is output. According to Eq. (22), the growth rate of the reluctance torque is greater than that of the permanent magnet torque with increasing current amplitude and angle. Therefore, the proportion of the permanent magnet torque is reduced, and the proportion of the reluctance torque is increased so that the output torque remains unchanged.

## V. PROTOTYPE AND EXPERIMENT

A prototype with 72 slots and 30 poles is developed to verify the rationality of the MCS-PMSM proposed in this paper. The specific parameters of the prototype are given in Table 3. The stator and rotor poles of the prototype are shown in Figs. 22 and 23. The experimental platform is shown in Fig. 24.

The output torque of the prototype with different numbers of modules put into operation is shown in Fig. 25. According to the simulation and test results, when the input current is fixed, the motor output torque increases linearly with the

**FIGURE 23.** Rotor poles.

**FIGURE 24.** The experimental platform.

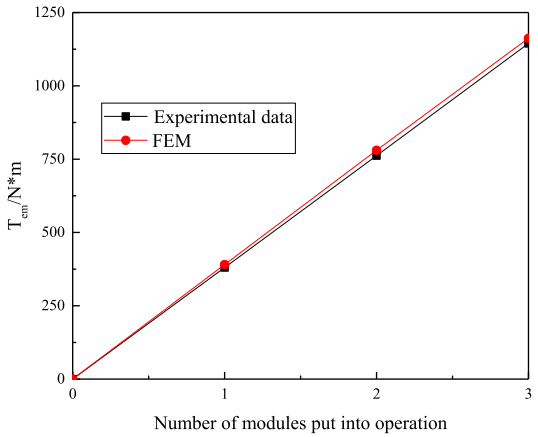


**FIGURE 25.** Output torque of the prototype with different numbers of modules put into operation.

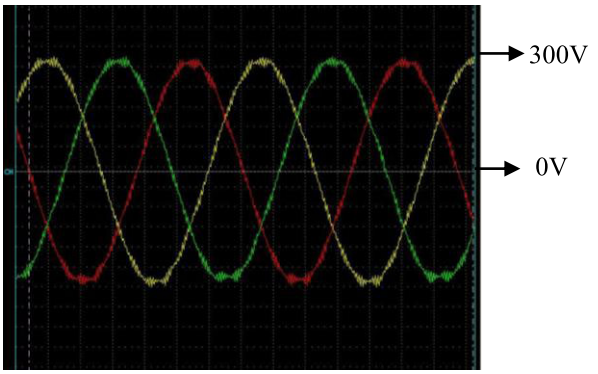


**FIGURE 26.** The no-load EMF waveform of the prototype.

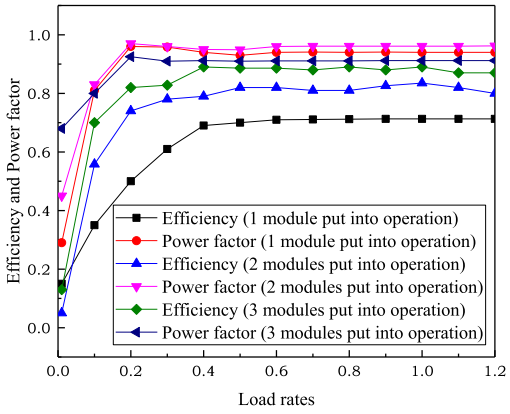


**FIGURE 27.** Efficiency and power factor of the prototype with different numbers of modules running at 60r/min.

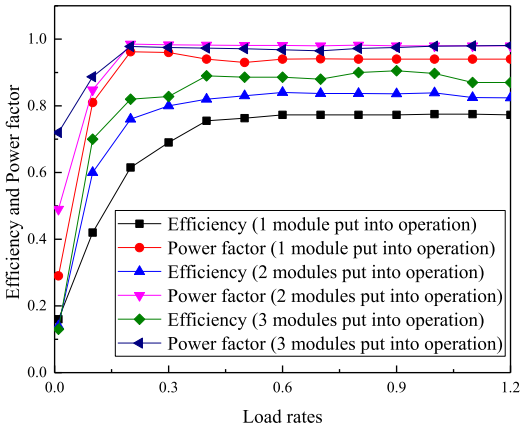


**FIGURE 28.** Efficiency and power factor of the prototype with different numbers of modules running at 80r/min.

number of modules put into operation, which is consistent with the results of mathematical model analysis. The measured value is slightly smaller than the simulation value. The reason is that the model is idealized during the simulation, and the no-load loss is not taken into account during the simulation.

As shown in Fig. 26, the measured back EMF is 213.3 V, and the simulated back EMF is 210.2 V. The error is only 1.4%.

In addition to the operation status evaluation of different modules at different load rates at rated speeds, the prototype is also measured at 60 r/min and 80 r/min. The results are shown in Figs. 27-29.

The results show that the efficiency of the MCS-PMSM decreases with a decrease in the number of modules when the load and speed of the motor are fixed.

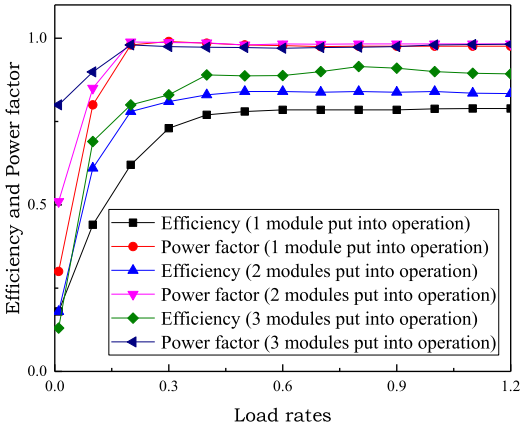


**FIGURE 29. Efficiency and power factor of the prototype with different numbers of modules running at 100r/min.**

When the load torque and speed of the motor are constant, the constant loss of the motor is essentially unchanged. The input electromagnetic power of the whole motor system is reduced with the reduction in the number of input modules. The motor system is equivalent to working in the overload state, and the efficiency of the MCS-PMSM is reduced due to the increasing copper loss brought by the increasing input current. The power factor changes little with different numbers of input modules. One reason is that the power factor of a PMSM is high because of the permanent magnet excitation, and the other reason is that the inverter has the function of reactive power compensation.

## VI. CONCLUSION

The MCS-PMSM is proposed to solve the complex problems of large-volume machining, transportation and maintenance of the low-speed and large-torque PMSM. First, the structure of the MCS and unequal span winding is described. The design rules of the MCS-PMSM are summarized. In the MCS-PMSM, the number of slots per pole and phase determines the minimum number of slots and pole pairs required for the unit modular motor, while the pole-slot matching determines the maximum number of independent operation modules and the maximum number of power supply branches of the whole motor system. The mathematical model of the MCS-PMSM is derived in the d-q coordinate system.

If one module fails to operate, other modules will operate in overload conditions, which will create unbalanced radial forces and increase the torque ripple. Under the fault operation state, the current of the machine can be reduced to the maximum extent by utilizing the reluctance torque of the tangential rotor structure.

The radial force acting on the stator is analyzed in the case of asymmetric operation. The FEM is used to analyze the normal and open-circuit fault operation of the MCS-PMSM, and the result shows that the MCS-PMSM has excellent performance in normal operation. Although the torque ripple and unbalanced radial force increase, the MCS-PMSM still has good fault tolerance in open-circuit faults and does not need a complex control system.

## REFERENCES

[1] F. Li, W. Hua, M. Tong, G. Zhao, and M. Cheng, "Nine-phase flux-switching permanent magnet brushless machine for low-speed and high-torque applications," *IEEE Trans. Magn.*, vol. 51, no. 3, pp. 1–4, Mar. 2015.

[2] J. M. Crider and S. D. Sudhoff, "An inner rotor flux-modulated permanent magnet synchronous machine for low-speed high-torque applications," *IEEE Trans. Energy Convers.*, vol. 30, no. 3, pp. 1247–1254, Sep. 2015.

[3] M. Valavi, J. Le Besnerais, and A. Nysveen, "An investigation of zeroth-order radial magnetic forces in low-speed surface-mounted permanent magnet machines," *IEEE Trans. Magn.*, vol. 52, no. 8, pp. 1–6, Aug. 2016.

[4] P. Arumugam, T. Hamiti, and C. Gerada, "Modeling of different winding configurations for fault-tolerant permanent magnet machines to restrain interturn short-circuit current," *IEEE Trans. Energy Convers.*, vol. 27, no. 2, pp. 351–361, Jun. 2012.

[5] Y. Fan, W. Zhu, X. Zhang, M. Cheng, and K. T. Chau, "Research on a single phase-loss fault-tolerant control strategy for a new flux-modulated permanent-magnet compact in-wheel motor," *IEEE Trans. Energy Convers.*, vol. 31, no. 2, pp. 658–666, Jun. 2016.

[6] X. Jiang, D. Xu, L. Gu, Q. Li, B. Xu, and Y. Li, "Short-circuit fault-tolerant operation of dual-winding permanent-magnet motor under the four-quadrant condition," *IEEE Trans. Ind. Electron.*, vol. 66, no. 9, pp. 6789–6798, Sep. 2019.

[7] S.-U. Chung, J.-W. Kim, Y.-D. Chun, B.-C. Woo, and D.-K. Hong, "Fractional slot concentrated winding PMSM with consequent pole rotor for a low-speed direct drive: Reduction of rare earth permanent magnet," *IEEE Trans. Energy Convers.*, vol. 30, no. 1, pp. 103–109, Mar. 2015.

[8] F. Sculiller, "Magnet shape optimization to reduce pulsating torque for a five-phase permanent-magnet low-speed machine," *IEEE Trans. Magn.*, vol. 50, no. 4, pp. 1–9, Apr. 2014.

[9] M. R. Shah and A. M. El-Refaie, "End effects in multiphase fractional slot concentrated-winding surface permanent magnet synchronous machines," *IEEE Trans. Energy Convers.*, vol. 25, no. 4, pp. 1001–1009, Dec. 2010.

[10] L. Alberti and N. Bianchi, "Experimental tests of dual three-phase induction motor under faulty operating condition," *IEEE Trans. Ind. Electron.*, vol. 59, no. 5, pp. 2041–2048, May 2012.

[11] F. Li, W. Hua, M. Cheng, and G. Zhang, "Analysis of fault tolerant control for a nine-phase flux-switching permanent magnet machine," *IEEE Trans. Magn.*, vol. 50, no. 11, pp. 1–4, Nov. 2014.

[12] J. Zhu, H. Bai, X. Wang, and X. Li, "Current vector control strategy in a dual-winding fault-tolerant permanent magnet motor drive," *IEEE Trans. Energy Convers.*, vol. 33, no. 4, pp. 2191–2199, Dec. 2018.

[13] B. Tian, G. Mirzaeva, Q.-T. An, L. Sun, and D. Semenov, "Fault-tolerant control of a five-phase permanent magnet synchronous motor for industry applications," *IEEE Trans. Ind. Appl.*, vol. 54, no. 4, pp. 3943–3952, Jul. 2018.

[14] W. Wang, J. Zhang, M. Cheng, and S. Li, "Fault-tolerant control of dual three-phase permanent-magnet synchronous machine drives under open-phase faults," *IEEE Trans. Power Electron.*, vol. 32, no. 3, pp. 2052–2063, Mar. 2017.

[15] B. Sen and J. Wang, "Stationary frame fault tolerant current control of poly-phase permanent magnet machines under open-circuit and short-circuit faults," *IEEE Trans. Power Electron.*, vol. 31, no. 7, pp. 4684–4696, Jul. 2016.

[16] W. Zhao, M. Cheng, K. T. Chau, W. Hua, H. Jia, J. Ji, and W. Li, "Stator-flux-oriented fault-tolerant control of flux-switching permanent-magnet motors," *IEEE Trans. Magn.*, vol. 47, no. 10, pp. 4191–4194, Oct. 2011.

[17] H. Zhou, J. Zhang, Z. Lu, X. Zhu, and M. Li, "A novel five-phase double-stator tubular fault-tolerant flux-modulation permanent magnet motor," *IEEE Trans. Appl. Supercond.*, vol. 28, no. 3, pp. 1–5, Apr. 2018.

[18] B. Wang, J. Wang, B. Sen, A. Griffo, Z. Sun, and E. Chong, "A fault-tolerant machine drive based on permanent magnet-assisted synchronous reluctance machine," *IEEE Trans. Ind. Appl.*, vol. 54, no. 2, pp. 1349–1359, Mar./Apr. 2018.

[19] W. Zhang, X. Liang, and F. Yu, "Fault-tolerant control of hybrid excitation axial field flux-switching permanent magnet machines," *IEEE Trans. Magn.*, vol. 54, no. 11, pp. 1–5, Nov. 2018.
[20] G. Yang, M. Lin, N. Li, G. Tan, and B. Zhang, "Flux-weakening control combined with magnetization state manipulation of hybrid permanent magnet axial field flux-switching memory machine," *IEEE Trans. Energy Convers.*, vol. 33, no. 4, pp. 2210–2219, Dec. 2018.
[21] L. Dong, Y. Huang, J. Jatskevich, and J. Liu, "Improved fault-tolerant control for brushless permanent magnet motor drives with defective Hall sensors," *IEEE Trans. Energy Convers.*, vol. 31, no. 2, pp. 789–799, Jun. 2016.
[22] Y.-P. Yang and M.-T. Peng, "A surface-mounted permanent-magnet motor with sinusoidal pulsewidth-modulation-shaped magnets," *IEEE Trans. Magn.*, vol. 55, no. 1, pp. 1–8, Jan. 2019.
[23] H. Li and Y. Shen, "Thermal analysis of the permanent-magnet spherical motor," *IEEE Trans. Energy Convers.*, vol. 30, no. 3, pp. 991–998, Sep. 2015.
[24] A. C. Malloy, R. F. Martinez-Botas, and M. Lamperth, "Measurement of magnet losses in a surface mounted permanent magnet synchronous machine," *IEEE Trans. Energy Convers.*, vol. 30, no. 1, pp. 323–330, Mar. 2015.
[25] S. Asgari and M. Mirsalim, "A novel dual-stator radial-flux machine with diametrically magnetized cylindrical permanent magnets," *IEEE Trans. Ind. Electron.*, vol. 66, no. 5, pp. 3605–3614, May 2019.
[26] W. Q. Chu and Z. Q. Zhu, "Average torque separation in permanent magnet synchronous machines using frozen permeability," *IEEE Trans. Magn.*, vol. 49, no. 3, pp. 1202–1210, Mar. 2013.
[27] H. N. Phyu, N. L. H. Aung, and C. Bi, "Influence of winding structure and the effect of MMF harmonics to the spindle motor performance for ultrahigh TPI HDD," *IEEE Trans. Magn.*, vol. 49, no. 6, pp. 2776–2781, Jun. 2013.
[28] S. Zuo, F. Lin, and X. Wu, "Noise analysis, calculation, and reduction of external rotor permanent-magnet synchronous motor," *IEEE Trans. Ind. Electron.*, vol. 62, no. 10, pp. 6204–6212, Oct. 2015.

**BINGYI ZHANG** received the B.S., M.S., and Ph.D. degrees in electrical engineering from the Shenyang University of Technology, Shenyang, China, in 1982, 1987, and 2007, respectively. He is currently a Professor with the Shenyang University of Technology. His research interests include design and optimization of electrical machines, low-speed high torque drive systems, and power system automation.

**BAOPING GAN** received the B.S. degree in electrical engineering and automation from the Shenyang University of Technology, Shenyang, China, in 2016, where he is currently pursuing the Ph.D. degree in electrical engineering. His research interest includes design and control of permanent magnet motor.

**QIAOSHAN LI** received the B.S. degree in electrical engineering and automation from the Shenyang University of Technology, Shenyang, China, in 2015, where she is currently pursuing the Ph.D. degree in electrical engineering. Her research interest includes design and analysis of electrical machines.